

Autonomous Navigation, Guidance and Control of Small Electric Helicopter

Regular Paper

Satoshi Suzuki^{1,*}, Takahiro Ishii², Nobuya Okada², Kojiro Iizuka¹ and Takashi Kawamura³¹ International Young Researchers Empowerment Center, Shinshu University, Japan² Graduate School of Science and Technology, Shinshu University, Japan³ Faculty of Textile and Technology, Shinshu University, Japan

* Corresponding author E-mail: s-s-2208@shinshu-u.ac.jp

Received 28 May 2012; Accepted 26 Oct 2012

DOI: 10.5772/54713

© 2013 Suzuki et al.; licensee InTech. This is an open access article distributed under the terms of the Creative Commons Attribution License (<http://creativecommons.org/licenses/by/3.0>), which permits unrestricted use, distribution, and reproduction in any medium, provided the original work is properly cited.

Abstract In this study, we design an autonomous navigation, guidance and control system for a small electric helicopter. Only small, light-weight, and inaccurate sensors can be used for the control of small helicopters because of the payload limitation. To overcome the problem of inaccurate sensors, a composite navigation system is designed. The designed navigation system enables us to precisely obtain the position and velocity of the helicopter. A guidance and control system is designed for stabilizing the helicopter at an arbitrary point in three-dimensional space. In particular, a novel and simple guidance system is designed using the combination of optimal control theory and quaternion kinematics. The designs of the study are validated experimentally, and the experimental results verify the efficiency of our navigation, guidance and control system for a small electric helicopter.

Keywords Autonomous control, Small Helicopter, Composite Navigation System, Low Accuracy Sensors, Three-Dimensional Guidance System

1. Introduction

In the last decade, unmanned aerial vehicle (UAV) technology has improved drastically, and UAVs are now used not only in research and development but also for various practical purposes such as aerial photography, surveillance and crop dusting. UAVs are safer and more convenient than manned aircraft and they can potentially have a wide range of applications. It is necessary to achieve autonomous control of UAVs in order to reduce operator burden in practical tasks. Therefore, several researchers have focused on the autonomous control of various types of UAVs such as fixed-wing UAVs [1] [2], helicopter-type UAVs [3]-[7], tilt-rotor-type UAVs [8], tail-sitter-type UAVs [9] and airship-type UAVs [10].

Recently, small UAVs weighing less than 10kg have attracted considerable attention owing to their ease of carriage and handling. Accordingly, we have investigated methods for achieving autonomous control of a 2 kg small electric helicopter. However, it is extremely difficult to achieve autonomous control of small helicopters

compared to large ones, owing to the payload limitation and sensor restriction. In general, larger sensors have greater accuracy. Hence, the sensors that can be mounted on 2 kg electric helicopters do not have enough accuracy for the requirements specification. Of course, some autopilot systems for small UAVs have already been proposed and developed [11]. However, in these autopilot systems, sensors are individually used to control each axis. For example, the *Inertial Measurement Unit* (IMU) is only used for attitude control, GPS for horizontal position and velocity control, and a barometer for height control. This configuration is not enough to control a small helicopter. In the case of a small helicopter, the accuracy and precision of a small GPS module is not enough for precise hovering and errors are caused in the barometer by down-wash from the rotor. These sensor errors should be compensated complementarily. Therefore, it is necessary for the autonomous control of a small helicopter to develop an integrated navigation system using multiple sensors. Meanwhile, the guidance system for small helicopters proposed in conventional works [3]-[7] is the full-state and coupling method. These methods are computationally expensive and not compatible with the small embedded computers that can be mounted on a 2 kg helicopter. Therefore, a simple and decoupled guidance method is desirable.

In this study, we design an autonomous navigation, guidance and control system for a small electric helicopter. There are two critical contributions in this paper. The first is an integrated navigation system using *Extended Kalman Filter* (EKF), and the second is a simple and decoupled guidance system. An integrated navigation system that consists of an inertial navigation, small, lightweight GPS module and a barometer are designed to obtain the accurate position and velocity of the helicopter. The guidance system is designed based on the combination of optimal control theory and quaternion kinematics. Flight experiments are conducted using a 2kg electric helicopter in order to validate the designed systems. Finally, accurate hovering and waypoint navigation of a small electric helicopter outdoors was achieved using a lightweight, inaccurate GPS module.

Source of power	Electric motor
Rotor diameter	955 mm
Body length	937 mm
Main rotor speed	1800 – 1900 rpm
Weight	1.6 kg
Payload capacity	1.0 kg

Table 1. Specifications of Lepton-Ex

2. Experimental Setup

This section introduces the experimental setup including the small electric helicopter and all sensors and electric devices for control of the helicopter



Figure 1. Lepton-Ex small electric helicopter

Fig.1 shows the small electric helicopter Lepton-Ex, and its specifications are listed in Table 1. Lepton-Ex was originally designed as a hobby-use radio-controlled helicopter by HIROBO. Co. Ltd. The configuration of a control device is shown in Table 2. The control device consists of a *Field Programmable Gate Array* (FPGA) board, a small attitude sensor that was designed in [12], a small light weight GPS module, a barometer, a photo-reflector module for measuring rotor revolution, and a wireless module. The configuration of our control device is similar to standard autopilot systems for small UAVs introduced in [11]. However, the sensors we use have a problem with their precision. Although larger sensors have greater accuracy and precision, large sensors could not be used because of the payload limitation of small electric helicopters. Hence, the sensors do not have enough accuracy for the control of the helicopter. In particular, we address the problem of a small GPS module. For the operation of an autonomous helicopter, for example for aerial photography, hovering precision of the helicopter has to be at least around 1.5 m in calm conditions. The hovering error comprises the control error and the sensor error. Therefore, the position error of the GPS module has to be smaller than 1.5 m. However, the small GPS module does not give such precision. An example of some data from a small GPS module is shown in Fig.2. The solid line represents the position data from the small GPS module and the dashed line represents ground truth data obtained by RTK-GPS, the precision of which is 2 mm. It is clear from Fig. 2 that the precision and accuracy of a small GPS module is not enough to meet the requirements specification. For this reason, we design a composite navigation system to compensate the GPS module error.

Main board	SUZAKU-V SZ410
Attitude sensor	IMU-05 by HIROBO
GPS module	u-blox LEA-6S
Barometer	SCP 1000
Photo reflector	BTE 003B
Wireless module	XBee-Pro
CPU core	PowerPC 405
CPU clock	350 MHz
OS	Linux 2.6
Weight (with box)	312 g

Table 2. Specifications of control device

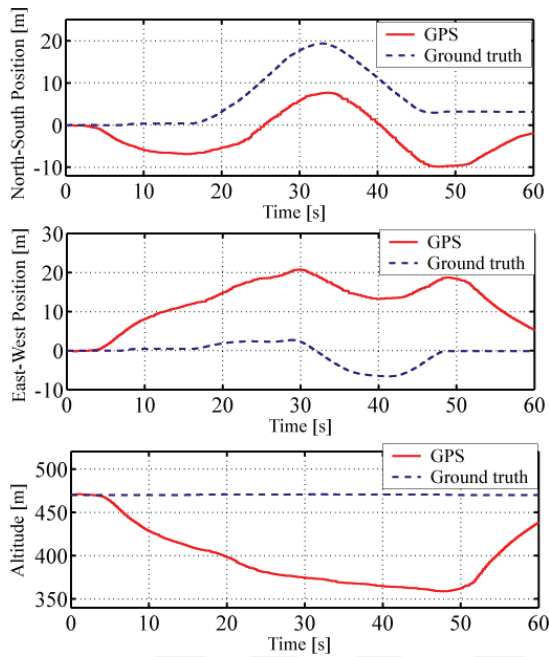


Figure 2. Data from small GPS module

3. Composite Navigation System

In this section, a composite navigation system consisting of an inertial navigation system, a barometric height measurement, and the small GPS module, is designed to compensate the error described in the previous section. We use EKF to integrate all sensor outputs. By using the composite navigation system, the outputs of each sensor are compensated complementarily, and accurate position and velocity data could be obtained as a result.

3.1 Coordinate Systems

First, we introduce the four coordinate systems used for designing the composite navigation system and specify the vector notation for each coordinate system. The first coordinate system is the inertial frame. It is denoted by *I-frame*; its origin is fixed at the centre of the Earth. Z_i indicates the Earth's polar axis; X_i and Y_i pass through points on the equator. The second coordinate system is the Earth frame, and is denoted by *E-frame*; its origin is fixed at the centre of the Earth similarly to *I-frame*. Z_e is the same as Z_i ; X_e passes through a point on the equator corresponding to 0deg longitude at any time, and rotates about Z_e in conjunction with the rotation of the Earth. The third coordinate system is the navigation frame, and is denoted by *N-frame*; its origin is fixed at the centre of gravity of the helicopter. X_n is aligned with the true north, Z_n with the direction of gravity, and Y_n with the east. In addition, the navigation algorithm is calculated in *N-frame*. The last coordinate system is the body frame, and is denoted by *B-frame*; its origin is at the centre of gravity of the helicopter. X_b is aligned with the forward direction of the body, Y_b with the rightward direction, and Z_b with the downward direction. The output of an accelerometer

is expressed as a vector in this frame (Fig.3). If an arbitrary vector in three-dimensional space is denoted by r , r is expressed in the frames defined above as r^i , r^e , r^n and r^b respectively.

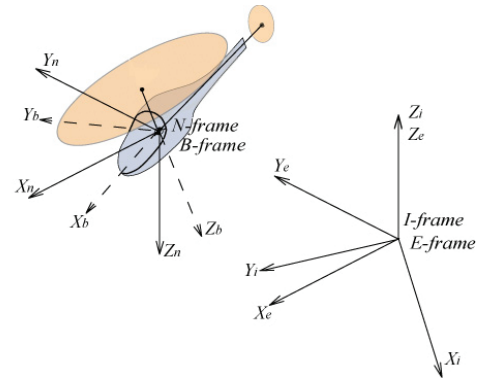


Figure 3. Coordinate system

3.2 Inertial Navigation

In this section, we present the derivation of the fundamental equations of inertial navigation. If V denotes the velocity vector of the helicopter, the navigation equation shown in [13] is obtained as

$$\dot{V}^n = f^n - (2\omega_{ie}^n + \omega_{en}^n) \times V^n + g^n \quad (1)$$

Generally, this equation holds not only for helicopters but for all moving bodies. Here, \times denotes the vector product and f^n is the acceleration vector. Components of f^n are expressed as $f^n = [a_n \ a_e \ a_d]^T$. Let $a^b = [a_x \ a_y \ a_z]^T$ denote the output of accelerometers mounted on the helicopter and let $R_n^b = [r_1^T \ r_2^T \ r_3^T]^T$ denote a matrix that expresses coordinate transformation from *B-frame* to *N-frame*. Then, the relation between f^n and a^b is obtained as

$$f^n = R_n^b a^b \quad (2)$$

where R_n^b is a 3×3 matrix, and r_1 , r_2 , and r_3 are 1×3 vectors. ω_{ie}^n in (1) is a vector in *N-frame*, which expresses the angular velocity of *E-frame* relative to *I-frame*. Considering the daily rotational angular velocity of the Earth as Ω_e , ω_{ie}^n is expressed as

$$\omega_{ie}^n = [\Omega_e \cos L \ 0 \ -\Omega_e \sin L]^T \quad (3)$$

Here, L denotes the latitude of the current position of the helicopter. ω_{en}^n is a vector in *N-frame*, which expresses the angular velocity of *N-frame* relative to *E-frame*. Considering the longitude of the current position of the helicopter as λ , ω_{en}^n is expressed as

$$\omega_{en}^n = [\dot{\lambda} \cos L \ -\dot{L} \ -\dot{\lambda} \sin L]^T \quad (4)$$

Lastly, g^n is the gravitational acceleration vector and is simply expressed as $g^n = [0 \ 0 \ g]^T$, where g is the

constant that expresses gravitational acceleration. Now, considering the components of the velocity vector as $\mathbf{V}^n = [v_n \ v_e \ v_d]^T$, (1) can be rewritten by using (2), (3), (4), and \mathbf{g}^n as follows:

$$\begin{aligned} \dot{v}_n &= \mathbf{r}_1 \mathbf{a}^b - 2v_e \Omega_e \sin L + v_d \dot{L} - \dot{\lambda} v_e \sin L \\ &\cong \mathbf{r}_1 \mathbf{a}^b - 2v_e \Omega_e \sin L \end{aligned} \quad (5)$$

$$\begin{aligned} \dot{v}_e &= \mathbf{r}_2 \mathbf{a}^b + (2\Omega_e + \dot{\lambda})(v_n \sin L + v_d \cos L) \\ &\cong \mathbf{r}_2 \mathbf{a}^b + 2\Omega_e (v_n \sin L + v_d \cos L) \end{aligned} \quad (6)$$

$$\begin{aligned} \dot{v}_d &= \mathbf{r}_3 \mathbf{a}^b - 2v_e \Omega_e \cos L - v_n \dot{L} - \dot{\lambda} v_e \cos L + g \\ &\cong \mathbf{r}_3 \mathbf{a}^b - 2v_e \Omega_e \cos L + g. \end{aligned} \quad (7)$$

Here, $\dot{\lambda}$ and \dot{L} in (5)-(7) are quite small because the range of flight is sufficiently narrow and the velocity of the helicopter is sufficiently small. Therefore, they can be neglected. If the semi-major axis and eccentricity of the Earth are denoted by R_l and e , respectively, the north-south directional radius of curvature R_n and the east-west directional radius of curvature R_e of the Earth are expressed as follows:

$$R_n = \frac{R_l(1-e^2)}{(1-e^2 \sin^2 L)^{3/2}}, \quad R_e = \frac{R_l}{(1-e^2 \sin^2 L)^{1/2}}. \quad (8)$$

According to [13], the time derivatives of latitude L , longitude λ , and altitude h are obtained by using R_n and R_e as follows:

$$\dot{L} = \frac{v_n}{R_n + h}, \quad \dot{\lambda} = \frac{v_e}{(R_e + h) \cos L}, \quad \dot{h} = -v_d. \quad (9)$$

Equations (5)-(7) and (9) are the fundamental equations of inertial navigation.

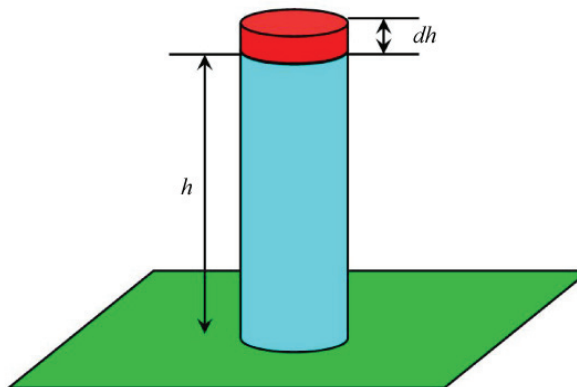


Figure 4. Air column

3.3 Barometric Height Measurement

GPS accuracy of height and vertical velocity is quite low compared to the horizontal position and velocity data. Therefore, error of vertical direction has to be

compensated by using additional sensors. In this study, we use a barometer to compensate the error, and in this section the relationship between the time derivatives of barometric pressure and the vertical velocity is derived for barometric height measurement. First, we consider an air column of height h , which is the same as the altitude of the helicopter (Fig.4); let ρ denote atmospheric density. Then, the relationship between the change in height dh and the change in air pressure dP is expressed as

$$dP = -\rho g dh. \quad (10)$$

Substituting the ideal gas law $\rho RT = MP$ into (10), we could obtain

$$RTdP = -MPgdh \quad (11)$$

where R is the gas constant, T is the air temperature, and M is the molar mass of the air. Now, we divide (11) by the micro time dt ; using the relationship between \dot{h} and v_d expressed in (9), the relationship between the time derivatives of the barometric pressure and the vertical velocity is derived as

$$\dot{P} = \frac{MP}{RT} g v_d. \quad (12)$$

In this equation, R , M , and g are constant; the air temperature T can be measured using the thermometer included in the MEMS barometer. Therefore, it is possible to calculate the vertical velocity on the basis of the change in barometric pressure.

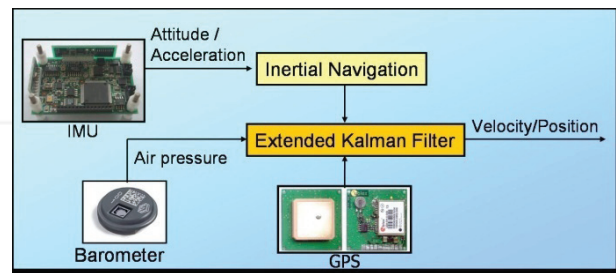


Figure 5. Block diagram of composite navigation system

3.4 Design of Extended Kalman Filter

In this section, we describe the design of the composite navigation system using the EKF. For designing EKF, a process model expressing the dynamics of the system is required. Therefore, we first derive the process model. The process model is derived on the basis of equations (5)-(7) and (9), inertial navigation and (12), and barometric height measurement. \mathbf{a}^b in (5)-(7) can be obtained using the small accelerometers mounted on the helicopter. However, output of small accelerometers includes a large bias error, resulting in the divergence of navigation computation. Therefore, in this case we assume that the bias error of the accelerometer has the

following dynamics; we introduce it into the process model, and finally compensate it.

$$\dot{b}_{ax} = w_x \quad \dot{b}_{ay} = w_y \quad \dot{b}_{az} = w_z. \quad (13)$$

Here, w_x , w_y , and w_z denote white noise. Introducing the vector $\mathbf{b}_a^b = [b_{ax} \ b_{ay} \ b_{az}]^T$, the true acceleration vector of the helicopter is obtained as $\mathbf{a}^b - \mathbf{b}_a^b$, and (2) could be rewritten as

$$\mathbf{f}^n = \mathbf{R}_b^n (\mathbf{a}^b - \mathbf{b}_a^b). \quad (14)$$

Therefore, (5)-(7) also could be rewritten, as follows:

$$\dot{v}_n = \mathbf{r}_1 (\mathbf{a}^b - \mathbf{b}_a^b) - 2v_e \Omega_e \sin L \quad (15)$$

$$\dot{v}_e = \mathbf{r}_2 (\mathbf{a}^b - \mathbf{b}_a^b) + 2\Omega_e (v_n \sin L + v_d \cos L) \quad (16)$$

$$\dot{v}_d = \mathbf{r}_3 (\mathbf{a}^b - \mathbf{b}_a^b) - 2v_e \Omega_e \cos L + g. \quad (17)$$

Integrating (9), (12), (13), and (15)-(17), the nonlinear state-space equation could be obtained as follows:

$$\begin{aligned} \dot{\mathbf{x}} &= \mathbf{f}(\mathbf{x}) + \mathbf{B}\mathbf{u} + \mathbf{G}\mathbf{w} \\ \mathbf{x} &= [L \ \lambda \ h \ v_n \ v_e \ P \ v_d \ b_{ax} \ b_{ay} \ b_{az}]^T \\ \mathbf{u} &= \mathbf{a}^b, \quad \mathbf{w} = [w_x \ w_y \ w_z] \end{aligned} \quad (18)$$

Digitizing the above equation, the discrete-time state-space equation could be obtained as

$$\mathbf{x}_{t+1} = \mathbf{f}_t(\mathbf{x}_t) + \mathbf{B}\mathbf{u}_t + \mathbf{G}\mathbf{w}_t \quad (19)$$

Next, the measurement equation is derived. Most of the small GPS module cannot output vertical velocity. Therefore, barometric pressure measured by the barometer is included in the output vector instead of the vertical velocity. Now, we consider the output vector of the system as $\mathbf{y}_t = [L \ \lambda \ h \ v_n \ v_e \ P]^T$, then, the measurement equation is derived as

$$\begin{aligned} \mathbf{y}_t &= \mathbf{H}_t \mathbf{x}_t + \mathbf{v}_t \\ \mathbf{H}_t &= [\mathbf{I}_{6 \times 6} \ \mathbf{0}_{6 \times 4}] \end{aligned} \quad (20)$$

Here, \mathbf{v}_t is the vector that expresses the measurement noise.

Now, let us consider $\hat{\mathbf{x}}_{t/t}$ to be the filtered estimate of \mathbf{x}_t , $\hat{\mathbf{x}}_{t/t-1}$ to be the predicted estimate of \mathbf{x}_t , and \mathbf{F}_t to be the state transition matrix, which can be calculated as

$$\mathbf{F}_t = \left(\frac{\partial \mathbf{f}_t(\mathbf{x}_t)}{\partial \mathbf{x}_t} \right)_{\mathbf{x}_t = \hat{\mathbf{x}}_{t/t}}. \quad (21)$$

The extended Kalman filter algorithm is obtained as follows:

$$\begin{aligned} \hat{\mathbf{x}}_{t/t-1} &= \mathbf{f}_{t-1}(\hat{\mathbf{x}}_{t-1/t-1}) \\ \mathbf{P}_{t/t-1} &= \mathbf{F}_{t-1} \mathbf{P}_{t-1/t-1} \mathbf{F}_{t-1}^T + \mathbf{G} \mathbf{Q}_{t-1} \mathbf{G}^T \\ \mathbf{K}_t &= \mathbf{P}_{t/t-1} \mathbf{H}_t^T [\mathbf{H}_t \mathbf{P}_{t/t-1} \mathbf{H}_t^T + \mathbf{R}_t]^{-1} \\ \hat{\mathbf{x}}_{t/t} &= \hat{\mathbf{x}}_{t/t-1} + \mathbf{K}_t [\mathbf{y}_t - \mathbf{H}_t \hat{\mathbf{x}}_{t/t-1}] \\ \mathbf{P}_{t/t} &= \mathbf{P}_{t/t-1} - \mathbf{K}_t \mathbf{H}_t \mathbf{P}_{t/t-1} \end{aligned} \quad (22)$$

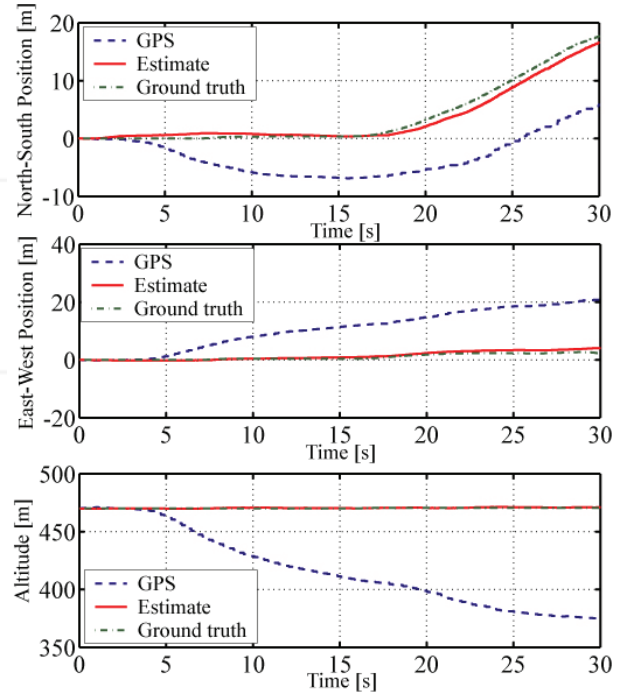


Figure 6. Validation result of composite navigation (position)

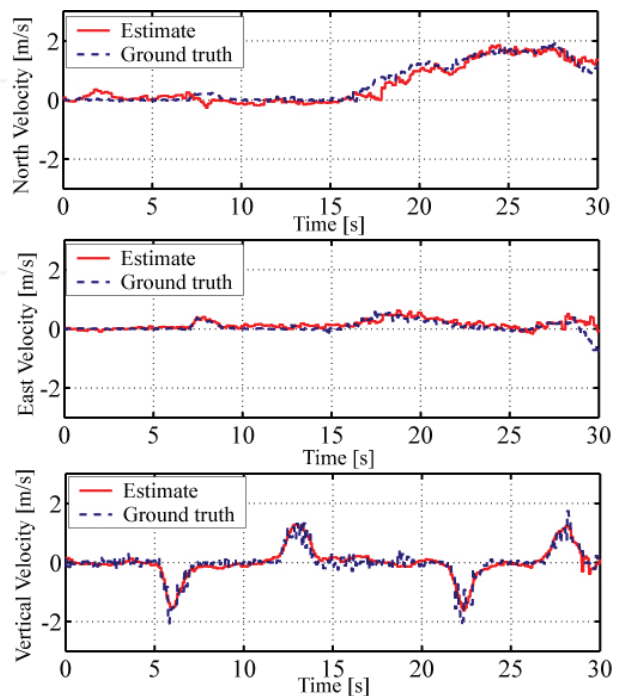


Figure 7. Validation result of composite navigation (velocity)

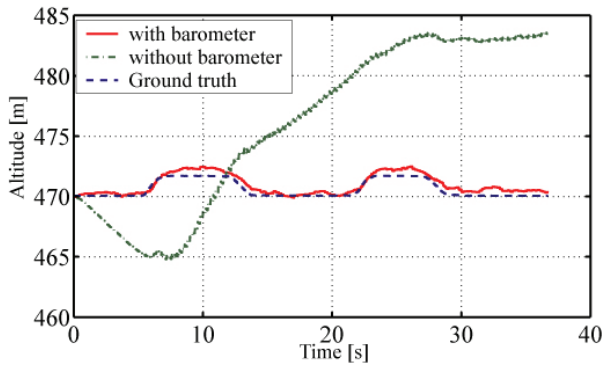


Figure 8. Comparison between With and Without barometer (altitude)

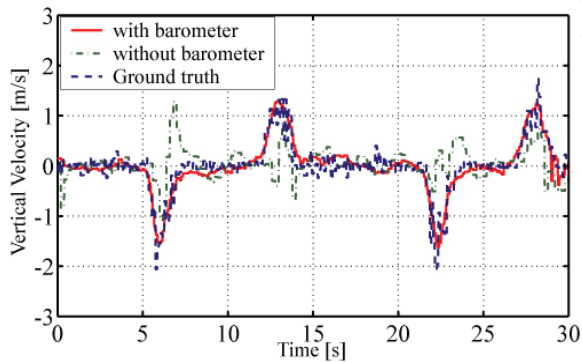


Figure 9. Comparison of data With and Without barometer (velocity)

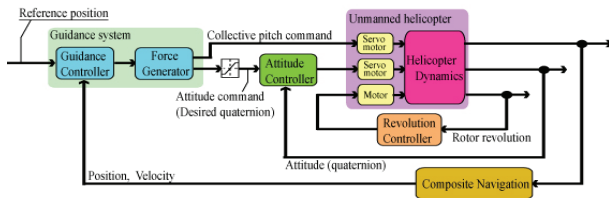


Figure 10. GNC system for small electric helicopter

Here, K_t is the Kalman gain, $P_{t/t}$ the covariance matrix about the estimation error, Q_t the covariance matrix for the system noise, and R_t the covariance matrix for the measurement noise. Finally, a block diagram of the entire system of composite navigation is shown in Fig.5.

3.5 Validation of Composite Navigation

To validate the designed composite navigation system, we carried out a validation experiment. In the experiment, whole devices including the GPS module were mounted on a cart, which was moved manually. An RTK-GPS was also mounted to obtain ground truth data. The navigation algorithm was calculated by using the computer embedded in the FPGA board. Fig.6 and Fig.7 show position and velocity data in the experiment. In these figures, the solid line represents the position and velocity data estimated by the composite navigation system. It is clear from Fig. 6 that the position was precisely estimated by the navigation system, even though the GPS data had a huge bias error in each axis.

Fig.7 shows that the velocity was also estimated precisely. Next, Fig.8 and Fig.9 show a comparison of the navigation result with barometric height measurement and without it. It is clear that altitude and vertical velocity data without barometric height measurement show significant error. This shows the effectiveness of a navigation system with barometric height measurement.

From the results, it can be concluded that the designed composite navigation system was able to estimate precise position and velocity, even though the GPS module showed significant error.

4. Guidance and Control System Design

In this section, we describe the design of the guidance and control system for the small electric helicopter. The block diagram of the entire guidance, navigation, and control (GNC) system is shown in Fig.10. The attitude controller was designed in previous studies [14] and [15] and composite navigation was designed in the previous section. Here, we realize the three-dimensional guidance of the helicopter. The helicopter performs translational motion by changing the magnitude and direction of the thrust of the main rotor, and it is equivalent to changing the collective pitch angle of the rotor blade and the attitude of the helicopter. Therefore, it is necessary to calculate the appropriate collective pitch angle and attitude for realizing the guidance of the helicopter. In the following, we design a rotor revolution controller and guidance system. The rotor revolution controller, which stabilizes the rotation speed of the main rotor, is designed to simplify the design of the guidance system. Next, the guidance system itself, which calculates the appropriate collective pitch angle and the attitude of the helicopter, is designed for stabilizing the helicopter at an arbitrary point in three-dimensional space.

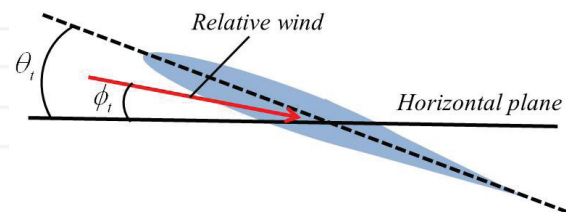


Figure 11. Definition of blade pitch angle and inflow angle

4.1 Rotor Revolution Control System

First, a mathematical model of the rotor revolution is derived for control system design. The source of power of our helicopter is an electric motor; therefore, we select the input voltage of the motor as the input and the angular velocity of the main rotor as the output. Table 3 lists the symbols used for model derivation. According to blade element theory [16], the resistance torque about the rotation axis of the rotor dQ , which is generated by blade element dr along the radius r of the blade, is expressed as

$$dQ = \frac{1}{2} \rho c r^3 \omega_r^3 \left\{ C_D - a \varphi_i \frac{R_r^2}{r^2} (\theta_i + \varphi_i) \right\} dr. \quad (23)$$

Resistance torque of rotor	Q	Nm
Drag coefficient	C_D	0.01
Angular velocity of rotor	ω_r	rad/sec
Input voltage to motor	v	V
Intensity of current	i	A
Torque of motor	τ	Nm
Motor resistance	R_m	1.0 Ω
Motor inductance	L_m	0.02 H
Moment of inertia of rotor	J	8.86×10^{-3} kgm ²
Viscous drag coefficient	μ	8.86×10^{-3} Nms/rad
Air density	ρ	1.205 kg/m ³
Blade chord length	c	0.04 m
Radius of rotor blade	R_r	0.478 m
Gear ratio	n	4
Back electromotive force constant	K_v	0.0107 Vs/rad
Torque constant of motor	K_τ	0.0107 Nm/A

Table 3. Notation for rotor modelling

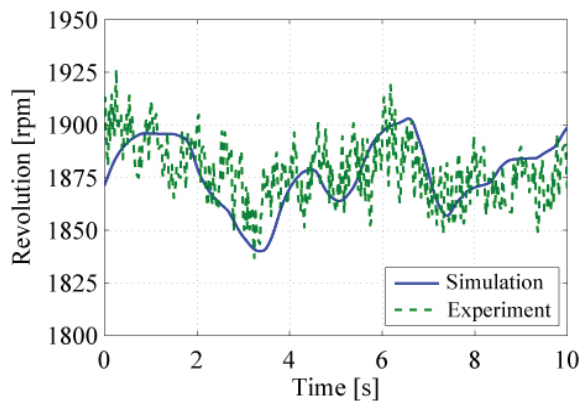


Figure 12. Validation result of rotor revolution model

Here, a is a two-dimensional lift curve slope and θ_i and φ_i are the blade pitch angle and the inflow angle at the blade tip (Fig.11). Considering that there are two blades, the total torque Q is obtained as

$$Q = 2 \int_0^{R_r} dQ = \frac{1}{4} \rho c R_r^4 \omega_r^2 \left\{ C_D - 2a \varphi_i (\theta_i + \varphi_i) \right\}. \quad (24)$$

Next, the system equation of the electric motor is derived. The circuit equation of the motor is expressed as

$$\begin{aligned} v &= R_m i + L_m \frac{di}{dt} + K_v n \omega_r \\ \tau &= K_\tau i. \end{aligned} \quad (25)$$

The equation of motion of the motor is expressed as

$$J n \dot{\omega}_r = \tau - \mu n \omega_r - Q \quad (26)$$

Here, the second term on the right-hand side represents the viscous drag. From (24)-(26), we obtain

$$\begin{aligned} v &= \frac{n J L_m}{K_\tau} \ddot{\omega}_r + \frac{n (J R_m + \mu L_m)}{K_\tau} \dot{\omega}_r + \left(\frac{\mu n R_m}{K_\tau} + K_v n \right) \omega_r \\ &+ \frac{\bar{C}_D \rho c R_r^4 L_m}{4 K_\tau} \dot{\omega}_r^2 + \frac{\bar{C}_D \rho c R_r^4 R_m}{4 K_\tau} \omega_r^2. \end{aligned} \quad (27)$$

Here, we consider \bar{C}_D in (27) as $\bar{C}_D = C_D - 2a \varphi_i (\theta_i + \varphi_i)$. Now, (27) is linearized around the hovering state. Assuming the angular velocity in the hovering state of Lepton-Ex is $\omega_{r0} = 193.5$ [rad/s], a small fluctuation in the angular velocity from the hovering state is defined as $\bar{\omega}_r = \omega_r - \omega_{r0}$. Using $\bar{\omega}_r$, (27) is linearized as follows:

$$\begin{aligned} v - v_0 &= \frac{n J L_m}{K_\tau} \ddot{\bar{\omega}}_r + \left\{ \frac{n (J R_m + \mu L_m)}{K_\tau} + \frac{\bar{C}_D \rho c R_r^4 L_m \omega_{r0}}{2 K_\tau} \right\} \dot{\bar{\omega}}_r \\ &+ \left(\frac{\mu n R_m}{K_\tau} + K_v n + \frac{\bar{C}_D \rho c R_r^4 R_m \omega_{r0}}{2 K_\tau} \right) \bar{\omega}_r \end{aligned} \quad (28)$$

Here, v_0 is the input voltage to the motor in the hovering state, and is obtained from (27) as

$$v_0 = \frac{\mu n R_m}{K_\tau} \omega_{r0} + K_v n \omega_{r0} + \frac{\bar{C}_D \rho c R_r^4 R_m}{4 K_\tau} \omega_{r0}^2. \quad (29)$$

Here, the first, second and fourth terms in (27) are zero because ω_{r0} is constant. Additionally, \bar{C}_D is assumed to be constant in the hovering state. If a small fluctuation in the input voltage from the hovering state is defined as $\bar{v} = v - v_0$, (28) could be transformed using Laplace transformation; then, rearranging the equation, the transfer function of the system is obtained as

$$G_r(s) = \frac{\bar{V}}{\bar{\Omega}_r} = \frac{K_1}{s^2 + K_2 s + K_3}. \quad (30)$$

Here, $\bar{\Omega}_r$ and \bar{V} are the Laplace transformations of $\bar{\omega}_r$ and \bar{v} , and constants K_1 , K_2 , and K_3 are obtained as

$$\begin{cases} K_1 = \frac{K_\tau}{n J L_m} \\ K_2 = \frac{R_m}{L_m} + \frac{\mu}{J} + \frac{\bar{C}_D \rho c R_r^4 \omega_{r0}}{2 n J} \\ K_3 = \frac{\mu R_m}{J L_m} + \frac{K_\tau K_v}{J L_m} + \frac{\bar{C}_D \rho c R_r^4 R_m \omega_{r0}}{2 n J L_m} \end{cases} \quad (31)$$

where R_m , L_m , J , and μ are unknown parameters in this model. In this study, we have determined the values of these unknown parameters by comparing the experimental data with the output of the model. The value of each parameter is listed in Table 3 and the comparison result is shown in Fig.12. The solid line represents the model output and the dashed line represents the rotor revolution data obtained in the experiment.

Next, the revolution controller is designed by using optimal control theory. First, the minimum realization of the transfer function (30) is derived as

$$\begin{aligned} \dot{\mathbf{x}}_r &= \mathbf{A}_r \mathbf{x}_r + \mathbf{B}_r u_r \\ y_r &= \mathbf{C}_r \mathbf{x}_r. \end{aligned} \quad (32)$$

Here, \mathbf{x}_r is defined as $\mathbf{x}_r = [\bar{\omega}_r \quad \dot{\bar{\omega}}_r]^T$. \mathbf{A}_r , \mathbf{B}_r , and \mathbf{C}_r are the system matrix, input matrix, and output matrix, respectively, defined as

$$\mathbf{A}_r = \begin{bmatrix} 0 & 1 \\ -K_3 & -K_2 \end{bmatrix} \quad \mathbf{B}_r = \begin{bmatrix} 0 \\ K_1 \end{bmatrix} \quad \mathbf{C}_r = [1 \quad 0]. \quad (33)$$

Now, the servo augmented system [17] is constructed as

$$\begin{bmatrix} \dot{\mathbf{x}}_r \\ \dot{e}_r \end{bmatrix} = \begin{bmatrix} \mathbf{A}_r & \mathbf{0} \\ -\mathbf{C}_r & 0 \end{bmatrix} \begin{bmatrix} \mathbf{x}_r \\ e_r \end{bmatrix} + \begin{bmatrix} \mathbf{B}_r \\ 0 \end{bmatrix} u_r + \begin{bmatrix} \mathbf{0} \\ 1 \end{bmatrix} \Omega_d \quad (34)$$

Here, Ω_d is desired angular velocity fluctuation from the hovering state and e_r is the integral of the error between desired and current angular velocity of the rotor. When we stabilize the angular velocity of the rotor to ω_{r0} , Ω_d could be set as zero. Considering $\bar{\mathbf{x}}_r$ as the state vector of the servo augmented system, we introduce the criterion

$$J_r = \int_0^\infty (\bar{\mathbf{x}}_r^T \mathbf{Q} \bar{\mathbf{x}}_r + R u_r^2) dt. \quad (35)$$

The feedback gain \mathbf{F}_r , which minimizes the criterion J_r , can be solved using optimal control theory and is obtained as

$$\mathbf{F}_r = \mathbf{R}^{-1} \mathbf{B}_r^T \mathbf{P}. \quad (36)$$

Here, \mathbf{P} is the solution of the following Riccati equation:

$$\mathbf{A}_r^T \mathbf{P} + \mathbf{P} \mathbf{A}_r - \mathbf{R}^{-1} \mathbf{P} \mathbf{B}_r \mathbf{B}_r^T \mathbf{P} + \mathbf{Q} = \mathbf{0}. \quad (37)$$

Using \mathbf{F}_r , the optimal control u_r can be calculated as

$$u_r = -\mathbf{F}_r \bar{\mathbf{x}}_r. \quad (38)$$

In addition, the state vector $\bar{\mathbf{x}}_r$ is estimated by the observer in the experiment because we can only measure the angular velocity of the rotor.

4.2 Guidance System

In this section, we design the guidance system for stabilizing the helicopter at an arbitrary point in three-dimensional space. The system is designed in two steps. First, we design a guidance controller that calculates the force vector required to stabilize the position and velocity of the helicopter. For simplicity, the helicopter could be considered as a point mass with inner loop dynamics. Second, we design a force generator that calculates the appropriate collective pitch angle of the rotor and the

reference attitude for achieving the desired force by using the rotor thrust.

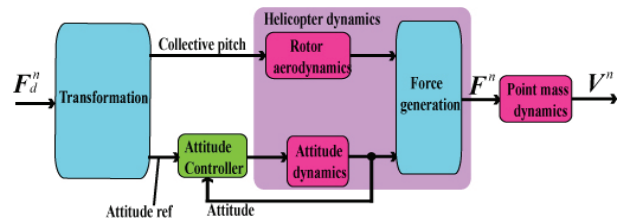


Figure 13. Translational dynamics of the helicopter

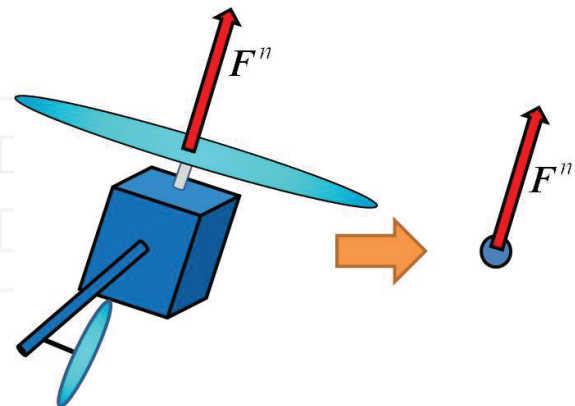


Figure 14. Point mass model

4.2.1 Guidance Controller

First, the mathematical model of the translational dynamics of the helicopter is derived. The entire system of the translational dynamics is shown in Fig.13. The input of the system is the desired force vector \mathbf{F}_d^n and the output is the three-dimensional velocity of the helicopter \mathbf{V}^n . Now, we assume that the dynamics between the force vectors \mathbf{F}^n and \mathbf{V}^n could be considered as point mass dynamics (Fig.14). Then, the equation of motion is obtained as

$$m \dot{\mathbf{V}}^n = \mathbf{F}^n - \mathbf{D}_v \mathbf{V}^n + m \mathbf{g}^n \quad (39)$$

where the mass of the helicopter is denoted by m . Additionally, the second term on the right-hand side represents attenuation term by air drag, and \mathbf{D}_v is the diagonal matrix expressing the damping factor of the air drag, defined as $\mathbf{D}_v = \text{diag}(d_v, d_v, d_v)$. (39) is expressed on N -frame. Originally, N -frame is not an inertial system; however, neglecting the effect of the Earth's rotation, N -frame can be considered as an inertial system. Considering $\mathbf{F}^n + m \mathbf{g}^n$ as the input of point mass dynamics, the transfer function of the point mass system for each axis could be obtained as

$$G_{pm}(s) = \frac{1}{ms + d_v}. \quad (40)$$

On the other hand, the dynamics between \mathbf{F}_d^n and \mathbf{F}^n are inner loop dynamics, such as the dynamics of the altitude

control system or rotor aero dynamics. We approximated these dynamics with a second order system. Then, the transfer function of inner loop dynamics could be obtained as

$$G_{in}(s) = \frac{k_{in}\omega_{in}^2}{s^2 + 2\zeta_{in}\omega_{in}s + \omega_{in}^2}. \quad (41)$$

Finally, using (40) and (41), the transfer function from \mathbf{F}_d^n to \mathbf{V}^n is obtained as follows:

$$G_v(s) = G_{pm}(s)G_{in}(s) = \frac{1}{ms + d_v} \frac{k_{in}\omega_{in}^2}{s^2 + 2\zeta_{in}\omega_{in}s + \omega_{in}^2}. \quad (42)$$

This transfer function was uniformly applied to each axis.

Next, the guidance controller is designed using the derived model, considering the latitude, longitude, and altitude of the target point as L_d , λ_d , and h_d respectively. Then, the velocity required to make the helicopter move to the target point is calculated, using proportional control as

$$\begin{aligned} v_{nd} &= K_{pn}(R_n + h)(L_d - L) \\ v_{ed} &= K_{pe}(R_e + h)\cos L(\lambda_d - \lambda) \\ v_{dd} &= -K_{pd}(h_d - h). \end{aligned} \quad (43)$$

Here, v_{nd} , v_{ed} and v_{dd} denote the desired velocities in the north, east, and downward directions, and K_{pn} , K_{pe} and K_{pd} denote the positive gain. Next, the velocity controller, which guarantees the velocity of the helicopter follows requirements, is designed using optimal control theory. First, the realization of the transfer function of (42) is expressed as

$$\begin{aligned} \dot{\mathbf{x}}_i &= \mathbf{A}_i \mathbf{x}_i + \mathbf{B}_i f_{di} \\ v_i &= \mathbf{C}_i \mathbf{x}_i \end{aligned} \quad (i = n, e, d). \quad (44)$$

The subscripts denote the direction (north, east, or downward); f_{di} is each axis component of \mathbf{F}_d^n . The servo augmented system is constructed as with (34). Considering the state of the servo augmented system as $\bar{\mathbf{x}}_i$, the feedback gain \mathbf{F}_i is obtained using optimal control theory. Then, the optimal control is calculated as

$$f_{di} = -\mathbf{F}_i \bar{\mathbf{x}}_i \quad (i = n, e, d). \quad (45)$$

An identity observer is designed for each axis to estimate unmeasured state in the experiment.

4.2.2 Force Generator

The force generator calculates the appropriate collective pitch angle of the main rotor and the desired quaternion [18] that expresses the attitude required to realize the

desired external force $\mathbf{F}_d^n = [f_{dn} \ f_{de} \ f_{dd}]^T$ using the thrust of the rotor. First, the collective pitch angle is calculated. Assuming that the rotation speed of the main rotor is stabilized by the revolution controller and is of constant value, the relationship between collective pitch angle δ_{pit} and the magnitude of the rotor thrust T_m is simply expressed from blade element theory as

$$T_m = K_T \delta_{pit}. \quad (46)$$

Here, K_T is a constant determined by the shape and rotation speed of the main rotor. Therefore, the collective pitch angle for achieving the desired external force could be obtained as

$$\delta_{pit} = \frac{|\mathbf{F}_d^n|}{K_T}. \quad (47)$$

Next, the quaternion that expresses the reference attitude is calculated. Now, we design a simple method for obtaining the desired quaternion using *Single Rotation* (SR) [18]. For the purposes of the design, the fifth coordinate system, reference frame, is defined. The reference frame is denoted by *R-frame*; its origin is fixed at the centre of gravity of the helicopter. Z_r is the same as Z_n . This frame rotates the desired heading angle of the helicopter, ψ_d , about Z_r (Fig.15). Considering the quaternion to express the attitude of *R-frame* relative to *N-frame* as \mathbf{q}_n^r , \mathbf{q}_n^r is obtained using SR as

$$\mathbf{q}_n^r = \left[\cos\left(\frac{\psi_d}{2}\right) \ 0 \ 0 \ \sin\left(\frac{\psi_d}{2}\right) \right]^T \quad (48)$$

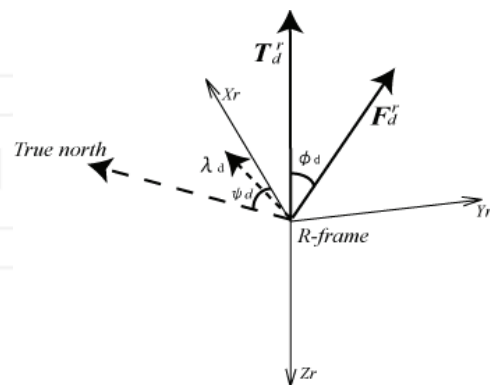


Figure 15. Definition of *R-frame*

According to [18], considering \mathbf{F}_d^r as the desired external force vector on *R-frame*, the relationship between \mathbf{F}_d^n and \mathbf{F}_d^r can be expressed as

$$\begin{bmatrix} 0 \\ \mathbf{F}_d^r \end{bmatrix} = \mathbf{q}_n^{r*} \otimes \begin{bmatrix} 0 \\ \mathbf{F}_d^n \end{bmatrix} \otimes \mathbf{q}_n^r. \quad (49)$$

Here, \otimes represents the quaternion product. Now, we define the desired thrust vector that indicates upward of

R -frame as $\mathbf{T}_d^r = \begin{bmatrix} 0 & 0 & -\mathbf{F}_d^r \end{bmatrix}^T$. Then, unit vector λ_d , which represents the rotation axis, and the rotation angle φ_d of SR that expresses the attitude to realize \mathbf{F}_d^r by using \mathbf{T}_d^r , could be obtained as

$$\lambda_d = \frac{\mathbf{T}_d^r \times \mathbf{F}_d^r}{\|\mathbf{T}_d^r \times \mathbf{F}_d^r\|}, \quad \varphi_d = \arcsin\left(\frac{\|\mathbf{T}_d^r \times \mathbf{F}_d^r\|}{\|\mathbf{T}_d^r\| \|\mathbf{F}_d^r\|}\right). \quad (50)$$

Using this SR, the quaternion \mathbf{q}_r^d that expresses the reference attitude relative to the attitude of R -frame is obtained as

$$\mathbf{q}_r^d = \left[c\left(\frac{\varphi_d}{2}\right) \quad \lambda_{dx}s\left(\frac{\varphi_d}{2}\right) \quad \lambda_{dy}s\left(\frac{\varphi_d}{2}\right) \quad \lambda_{dz}s\left(\frac{\varphi_d}{2}\right) \right]^T \quad (51)$$

where $c(x) = \cos x$ and $s(x) = \sin x$, λ_{dx} , λ_{dy} , and λ_{dz} are the components of λ_d along each axis. Finally, the desired quaternion \mathbf{q}_n^d , which expresses the reference attitude, is calculated using \mathbf{q}_r^d and \mathbf{q}_n^r as follows:

$$\mathbf{q}_n^d = \mathbf{q}_n^r \otimes \mathbf{q}_r^d. \quad (52)$$

The desired external force could be achieved by using (47),(52) and the attitude control system designed in previous studies.

5. Experiments

Experiments were carried out to validate the proposed guidance and control systems. The results are presented in the following sections. The parameters used for the design of the guidance and control system are listed in Table 4.

Rotor revolution control		
$\mathbf{Q} = \text{diag}(100 \quad 1 \quad 2000)$	$R = 1$	
Velocity control		
	Horizontal	Vertical
ω_{in}	$2\pi \times 0.055$ rad/s	$2\pi \times 0.028$ rad/s
ζ_{in}	1.5	1.5
k_{in}	2.5	2.5
m	2.6 kg	2.6 kg
d_v	6.19 Ns/m	6.19 Ns/m
\mathbf{Q}	$\text{diag}(75 \quad 1 \quad 50 \quad 200)$	$\text{diag}(10 \quad 5 \quad 1 \quad 7)$
R	10	20
Position control		
$K_{pn} = 0.2$	$K_{pe} = 0.2$	$K_{pd} = 0.2$

Table 4. Design parameter

5.1 Rotor Revolution Control Experiment

First, the revolution control experiment was carried out on the ground. In this experiment, the helicopter was stationary on the ground and the rotor revolution

reference was expressed by a step signal. Fig.16 shows the result of the experiment. The solid line represents the rotor revolution measured by the photo reflector module, and the dashed line represents the reference revolution. This figure clearly shows that the rotor revolution precisely follows the reference revolution.

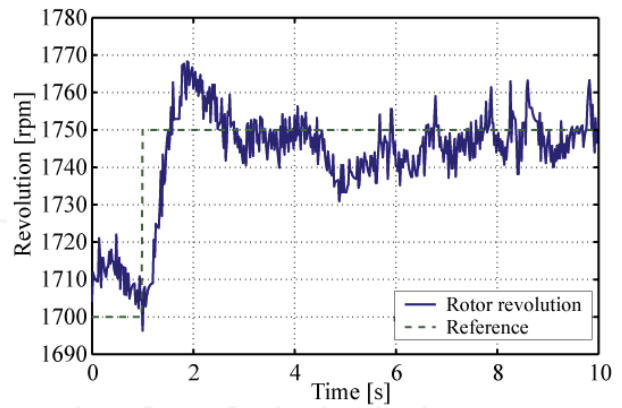


Figure 16. Revolution control on the ground

Next, a flight experiment was carried out. In this experiment, only the rotor revolution was controlled, and the other axis was controlled manually. In addition, the reference revolution was expressed as a constant because it is necessary to stabilize the rotor revolution to a constant value for (46). The result is shown in Fig.17 and Fig.18.

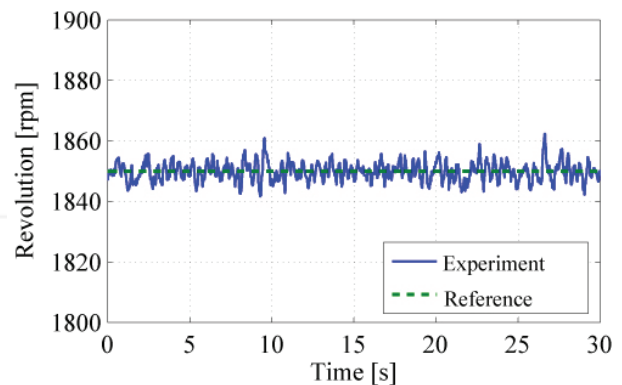


Figure 17. Revolution control in flight (revolution)

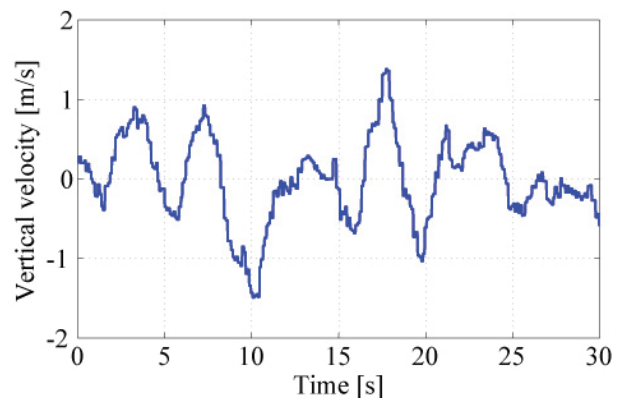


Figure 18. Revolution control in flight (vertical velocity)

Fig.17 shows the rotor revolution and Fig.18 shows the vertical velocity. The rotor revolution could be stabilized to a constant value even if the helicopter moved upward (10 s) or downward (17 s). From the result, the rotor revolution can be considered as constant in flight, and so the assumption for (46) could be satisfied.

5.2 Guidance Control Experiment

Finally, three-dimensional guidance control experiments were carried out. The experiments were conducted outdoors. The average wind speed was approximately 1-2 m/s. Fig.19 and Fig.20 show the 3-D and 2-D trajectories in the hovering experiment. The reference position has been fixed at the origin. The figure shows that 95% of the entire flight trajectory was included in the 0.5 m ball centred at the origin.

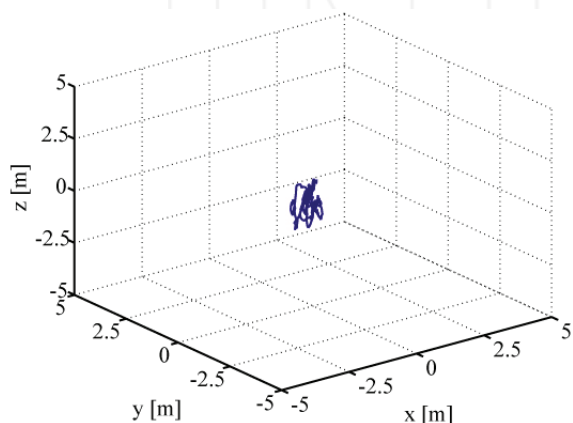


Figure 19. Hovering experiment (three-dimensional trajectory)

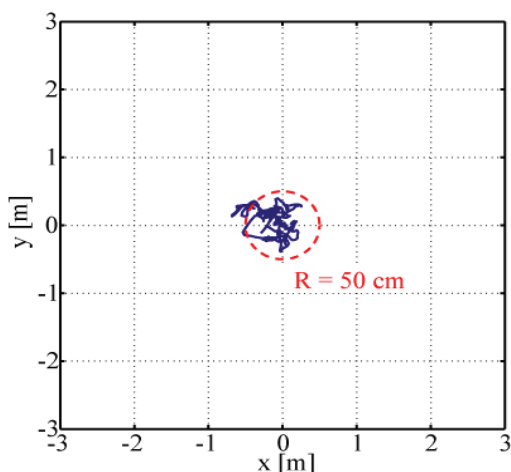


Figure 20. Hovering experiment (two-dimensional trajectory)

Fig.21 and Fig.22 show the horizontal and vertical trajectories of waypoint flight. In this experiment, the waypoint was expressed from a ground station via wireless communication. The figure clearly shows that the helicopter accurately passed each waypoint both horizontally and vertically.

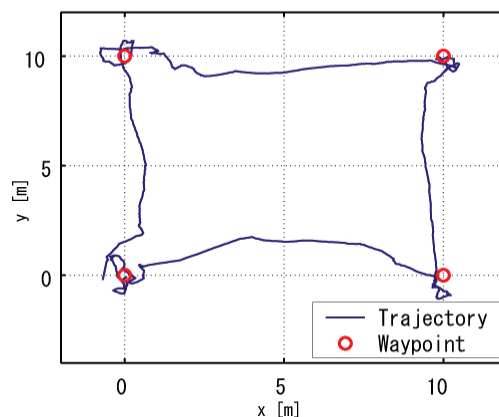


Figure 21. Waypoint flight

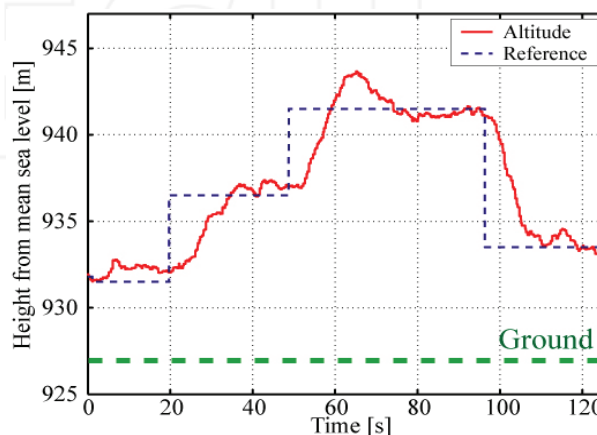


Figure 22. Altitude control

From the results, it can be said that the hovering error is < 1.5 m, and so the navigation, guidance and control system designed in this paper satisfy the requirements specification for an autonomous helicopter.

6. Conclusion

In this paper, we presented the design of a composite navigation system and a three-dimensional guidance and control system for a small electric helicopter. A novel composite navigation system was developed using an inertial navigation, a barometric height measurement, and an inaccurate GPS module. A simple method was suggested for calculating the reference attitude and the collective pitch angle of the main rotor in order to realize three-dimensional guidance of the helicopter. The experimental results verified the effectiveness of the proposed navigation, guidance and control systems. In the future, we plan to realize automated take-off and landing and to achieve fully autonomous cooperative control of multiple helicopters.

7. References

- [1] C. K. Oh and G. J. Barlow, "Autonomous Controller Design for Unmanned Aerial Vehicles using Multi-object Genetic Programming," in *Proceedings of*

- Congress on Evolutional Computation 2004*, vol. 2, pp. 1538-1545, 2004.
- [2] J. M. Eklund, J. Sprinkle and S. Sastry, "Implementing and Testing a Nonlinear Model Predictive Tracking Controller for Aerial Pursuit/Evasion Games on a Fixed Wing Aircraft," in *Proceedings of 2005 American Control Conference*, vol. 3, pp. 1509-1514, 2005.
- [3] B. Mettler, "System Identification Modeling of a Small-Scale Unmanned Rotorcraft for Flight Control Design," *Journal of American Helicopter Society*, vol. 47, no. 1, pp. 50-63, 2002.
- [4] H. J. Kim and D. H. Shim, "A Flight Control System for Aerial Robots: Algorithm and Experiment," *Journal of Control Engineering Practice*, vol. 11, pp. 1389-1400, 2003.
- [5] N. J. Eric, K. K. Suresh and K. Kannan, "Adaptive Trajectory Control for Autonomous Helicopters," *AIAA Journal Guidance Control and Dynamics*, vol. 28, no. 3, pp. 524-538, 2005.
- [6] C. L. Castillo, W. Alvis, M. Castillo-Effen, W. Moreno and K. Valavanis, "Small Unmanned Helicopter Simplified and Decentralized Optimization-based Controller Design for Non-aggressive Flights," *International Journal on Systems Science and Applications*, vol. 1, no. 3, pp. 303-315, 2006.
- [7] S. Shen, N. Michael and V. Kumar, "Autonomous Multi-floor Indoor Navigation with a Computationally Constrained MAV," in *Proceedings of IEEE International Conference on Robotics and Automation 2011*, pp. 20-25, 2011.
- [8] J. H. Lee, B. M. Min and E. T. Kim, "Autopilot Design of Tilt-rotor UAV using Particle Swarm Optimization Method," in *Proceedings of the 2007 International Conference of Control, Automation and Systems*, pp. 1629-1633, 2007.
- [9] H. Stone and K. C. Wong, "Preliminary Design of a Tandem-wing Tail-sitter UAV using Multi-disciplinary Design Optimization," in *Proceedings of International Aerospace Congress*, pp. 707-720, 1997.
- [10] S. J. Lee, S. P. Kim, T. S. Kim, H. K. Kim and H. C. Lee, "Development of Autonomous Flight Control System for 50 m Unmanned Airship," in *Proceedings of 2004 Intelligent Sensors, Sensor Networks Information Processing Conference*, pp. 457-461, 1997.
- [11] H. Chao, Y. Cao and Y. Chen, "Autopilots for Small Unmanned Aerial Vehicles: A Survey," *International Journal of Control, Automation, and Systems*, vol. 8, no. 1, pp. 36-44, 2010.
- [12] S. Suzuki, M. Tawara, D. Nakazawa and K. Nonami, "Research on Attitude Estimation Algorithm under Dynamic Acceleration," *Journal of the Robotics Society of Japan*, vol. 26, no. 6, pp. 626-634, 2008, (in Japanese).
- [13] R. M. Rogers, *Applied Mathematics in Integrated Navigation System, Second Edition*, Reston: AIAA Education Series, 2003.
- [14] S. Suzuki, D. Nakazawa, K. Nonami and M. Tawara, "Attitude Control of Small Electric Helicopter by using Quaternion-Feedback," *Journal System Design and Dynamics*, vol. 5, no. 2, pp. 231-247, 2011.
- [15] S. Suzuki and K. Nonami, "Nonlinear Adaptive Control for Small-Scale Helicopter," *Journal of the Robotics Society of Japan*, vol. 5, no. 5, pp. 866-880, 2011.
- [16] A.R.S. Bramwell, G. Done and D. Balmford, *Bramwell's Helicopter Dynamics, Second Edition*, Reston: AIAA, 2001.
- [17] W. M. Wonham, *Linear Multivariable Control –A Geometric Approach*, New York: Springer-Verlag, pp. 203-210, 1978.
- [18] J. B. Kuipers, *Quaternions and Rotation Sequences*, Princeton: Princeton University Press, 2002.

INTECH